Journal of Coordination Chemistry

ISSN: 0095-8972 (Print) 1029-0389 (Online) Journal homepage: http://www.tandfonline.com/loi/gcoo20

Syntheses, characterizations, crystal structures, and biological activities of two new mixed ligand Ni(II) and Cu(II) Schiff base complexes

S. Yousef Ebrahimipour, Maryam Mohamadi, Jesús Castro, Nasrin Mollania, Hadi Amiri Rudbari & Alessandro Saccá

To cite this article: S. Yousef Ebrahimipour, Maryam Mohamadi, Jesús Castro, Nasrin Mollania, Hadi Amiri Rudbari & Alessandro Saccá (2015) Syntheses, characterizations, crystal structures, and biological activities of two new mixed ligand Ni(II) and Cu(II) Schiff base complexes, Journal of Coordination Chemistry, 68:4, 632-649, DOI: 10.1080/00958972.2014.1000883

To link to this article: http://dx.doi.org/10.1080/00958972.2014.1000883

Accepted author version posted online: 23 Dec 2014.
Published online: 20 Jan 2015.

Journal of Coordination Chemistry, 2015
Vol. 68, No. 4, 632–649, http://dx.doi.org/10.1080/00958972.2014.1000883

Syntheses, characterizations, crystal structures, and biological activities of two new mixed ligand Ni(II) and Cu(II) Schiff base complexes

S. YOUSEF EBRAHIMIPOUR*†, MARYAM MOHAMADI†, JESÚS CASTRO‡, NASRIN MOLLANIA§, HADI AMIRI RUDBARI¶ and ALESSANDRO SACCÁ‖

†Department of Chemistry, Faculty of Science, Shahid Bahonar University of Kerman, Kerman, Iran
‡Departamento de Química Inorgánica, Universidade de Vigo, Facultade de Química, Edificio de Ciencias Experimentais, 36310 Vigo, Galicia, Spain
§Department of Biology, Faculty of Basic Sciences, Hakim Sabzevari University, Sabzevar, Iran
¶Faculty of Chemistry, University of Isfahan, Isfahan, Iran
‖Dipartimento di Scienze Chimiche, Universita´ di Messina, Messina, Italy

(*Received 30 August 2014; accepted 4 December 2014*)

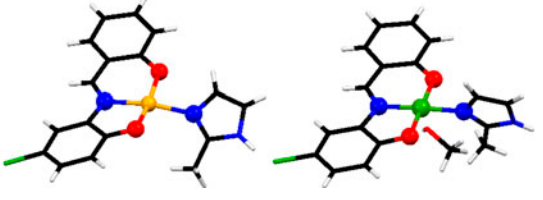

Two mixed-ligand complexes, [Cu(L)(2imi)] (**1**) and [Ni(L)(2imi)]·MeOH (**2**) [L = 2-(((5-chloro-2-oxyphenyl)imino)methyl)phenolato) and 2imi = 2-methyl imidazole], have been prepared by the reaction of appropriate metal salts with H_2L and 2-methyl imidazole. Their structures were characterized by microanalysis, FT-IR, UV–vis, molar conductivity, and ^{1}H NMR for [Ni(L)(2imi)]·MeOH. The structures were determined using single crystal X-ray diffraction. Each four-coordinate metal center, Cu(II) in **1** and Ni(II) in **2**, is surrounded by donors of Schiff base (L^{2-}) and N of 2-methyl imidazole in square planar geometries. α-Amylase activities of these compounds have also been investigated. The experimental data showed that α-amylase was inhibited by Ni(II) complex while the Cu(II) complex causes a 1.3-fold decrease in K_m value. Antimicrobial results show that these compounds, especially the Cu(II) complex, have potential for antibacterial activity against Gram negative and Gram positive bacteria and antifungal activity against *Aspergillus fumigatus*.

Keywords: Schiff base; Ni(II) complex; Cu(II) complex; Anti-microbial activity; α-Amylase activity; Enzyme inhibitory

1. Introduction

Asymmetric Schiff bases, especially ONO tridentate ones, have attracted much attention because of structural similarities with some biological units, their facile synthesis, and applications in different areas [1, 2].

*Corresponding author. Email: Ebrahimipour@uk.ac.ir

These compounds form various complexes with metal ions in different oxidation states. Among these, there has been increasing interest in research in Cu(II) and Ni(II) complexes due to their applications in various fields [3, 4]. They are widely used in industrial processes [5, 6]. Investigation of their biological properties has been of more importance, since in many cases, complexation can improve these properties of the resultant compounds [7, 8]. Furthermore, copper exists in biological systems with asymmetric multidentate chelates [9, 10]. Many Cu(II) Schiff base complexes are models for simulating and representing the function of copper ion in copper-containing proteins and enzymes such as polyphenol oxidase [11]. Cu(II) complexes containing ONO Schiff base ligands reveal other biological properties such as DNA binding, anti-cancer, anti-oxidant, and anti-microbial activities [12–15].

Nickel also plays a role in some redox enzymes such as urease [16]. Similar to Cu, Ni (II)–ONO Schiff base complexes possess considerable biological activities [17–19].

On the other hand, α-amylase, an enzyme existing in plants, animals, and microorganisms, cleaves internal α-1,4-glycosidic linkages [20]. α-Amylase inhibitors reduce postprandial hyperglycemia by partially inhibiting the enzymatic hydrolysis of complex carbohydrates, and, hence, delay the absorption of glucose. Accordingly, α-amylase inhibitors are used as targets for drug-designing in the treatment of diabetes, obesity, and hyperlipidemia [21]. Herein, we describe the synthesis, characterization, α-amylase inhibitory, and antimicrobial activities of two new square-planar mixed-ligand Ni(II) and Cu(II) complexes with tridentate ONO salicylidene derivative ligand and 2-methyl imidazole.

2. Experimental

2.1. *Materials and instrumentation*

All chemicals were analytical grade and used as received. [H_2L] was prepared according to our previous report [22]. Elemental analyses of C, H, and N were performed on a Perkin Elmer 2400 CHNS/O elemental analyzer. The FT-IR spectrum was recorded on a Nicolet-Impact 400D spectrometer (4000–400 cm^{-1}) in KBr pellets. Conductance measurements were made with a Metrohm 712 Conductometer in DMSO. ^1H NMR spectrum was recorded at 25 °C with a Bruker BRX 100 AVANCE spectrometer. The electronic spectra were recorded in DMSO on a Cary 50 spectrophotometer. Melting point was determined on a Gallenkamp melting point apparatus.

2.2. *Synthesis of 2-(((5-chloro-2-hydroxyphenyl)imino)methyl)phenol [H_2L]*

Ethanolic solution (5 mL) of 2-amino-4-chlorophenol (0.3 g, 2 mmol) was added to an ethanolic solution (5 mL) of 2-hydroxy-benzaldehyde (0.2 g, 2 mmol) with vigorous stirring. After 15 min heating, the solution was cooled and an orange precipitate was separated by filtration, washed with cold ethanol, and dried in a desiccator over anhydrous $CaCl_2$. Yield: 0.41 g, 83%. M.p.: 156 °C. Anal. Calcd for $C_{13}H_{10}ClNO_2$ (247.68 g mol^{-1}): C, 63.04; H, 4.07; N, 5.66. Found: C, 63.18; H, 4.01; N, 5.73%. FT-IR (KBr) cm^{-1}: ν(OH) 3047, ν(C=N) 1627, ν(C=C_{ring}) 1496, ν(C–O) 1307, ν(C–Cl) 655. ^1H NMR (100 MHz, DMSO-d_6, 25 °C, ppm): δ = 13.4 (s, 1H; OH), 10 (s, 1H; OH), 9.0 (s, 1H; CH=N), 6.7–7.8 (m, 7H, rings). UV/Vis (DMSO) λ_{max}, nm (log(ε), L mol^{-1} cm^{-1}): 271(4.41), 361(4.31), 460(4.24).

2.3. *(2-Methylimidazole)(2-(((5-chloro-2-oxyphenyl)imino)methyl)phenolato))copper(II) [Cu(L)(2imi)] (1)*

Methanolic solution (4 mL) of $Cu(NO_3)_2{\cdot}4H_2O$ (0.1 mmol, 0.02 g) was added to 3 mL solution of H_2L (0.1 mmol, 0.03 g) and NaOH (0.2 mmol, 0.01 g) with constant stirring and the mixture was refluxed in a water bath for 5 min. Then, 4 mL methanolic solution of 2-methyl imidazole (0.3 mmol, 0.02 g) was added to the reaction mixture and the reflux was continued for an additional 2 h. With slow evaporation of the resulting solution, red crystals appeared. These were separated, dried in air at room temperature, and stored in a $CaCl_2$ desiccator. Yield: 0.022 g, 56%. M.p.: 206 °C. Molar conductance (10^{-3} M, DMSO) 23.0 Ω^{-1} cm^2 mol^{-1}. Anal. Calcd for $C_{17}H_{14}ClCuN_3O_2$ (391.31 g mol^{-1}): C, 52.18; H, 3.61; N, 10.74. Found: C, 52.24; H, 3.48; N, 10.80%. FT-IR (KBr) cm^{-1}: ν(NH) 3421, ν(C=N) 1608, ν(C=C$_{ring}$) 1473, ν(C–O) 1281, ν(C–Cl) 651. UV/Vis (DMSO, λ_{max}, nm (log (ε), L mol^{-1} cm^{-1}): 306(3.92), 399(2.85), 450(3.06), 661(2.18).

2.4. *(2-Methylimidazole)(2-(((5-chloro-2-oxyphenyl)imino)methyl)phenolato))nickel(II) methanol solvate [Ni(L)(2imi)]·MeOH (2)*

$Ni(NO_3)_2{\cdot}4H_2O$ (0.1 mmol, 0.02 g) was added to 4 mL methanolic solution of H_2L (0.1 mmol, 0.018 g) and the resulting brown mixture was refluxed in a water bath for 10 min. To the mixture, 2-methyl imidazole (0.3 mmol, 0.02 g) was added, giving a reddish solution that was further refluxed for *ca*. 40 min. After cooling, the precipitate was separated and then recrystallized from ethanol–methanol (30/70%) to give red single crystals that were dried in a vacuum desiccator over $CaCl_2$. Yield: 0.027 g, 64%. M.p.: 211 °C. Molar conductance (10^{-3} M, DMSO) 28.0 Ω^{-1} cm^2 mol^{-1}. Anal. Calcd for $C_{18}H_{18}ClN_3NiO_3$ (418.50 g mol^{-1}): C, 51.66; H, 4.34; N, 10.04. Found: C, 51.81; H, 4.25; N, 10.15%. FT-IR (KBr) cm^{-1}: ν(NH) 3419, ν(OH) 3101, ν(C=N) 1608, ν(C=C$_{ring}$) 1481, ν(C–O) 1284, ν(C–Cl) 675. ^{1}H NMR (100 MHz, DMSO-d_6, ppm): δ = 12.8 (*s*, 1H, NH), 9.7 (*s*, 1H; CH=N), 6.7–8.1 (*m*, 9H; rings), 3.9 (*q*, H; OH), 3.2 (*d*, 3H; CH_3), 2.9 (s, 3H, CH_3). UV/Vis (DMSO, λ_{max}, nm (log(ε), L mol^{-1} cm^{-1}): 305(3.81), 401(3.90), 454(4.16).

2.5. *Crystal structure determination*

X-ray data were collected at room temperature with a Bruker APEX II CCD area-detector diffractometer using Mo Kα radiation (λ = 0.71073 Å). Data collection, cell refinement, data reduction, and absorption correction were performed using multi-scan methods with Bruker software [23]. The structures were solved by direct methods using SIR2004 [24]. The non-hydrogen atoms were refined anisotropically by full matrix least squares on F^2 using SHELXL 97 [25]. All hydrogens except N–H and O–H hydrogens were placed in calculated positions and refined as isotropic with the "riding-model technique". Hydrogens of N–H and O–H were found in a difference Fourier map and refined isotropically with distance restraints of N–H = 0.86 Å and N–H = 0.82 Å. The complete conditions for data collection and structure solution are given in table 1.

2.6. *α-Amylase activity determination and biochemical characterization*

α-Amylase activity was assessed at 37 °C using potato starch (1%) as a substrate in 20 mM Tris–HCl, pH 7.4. The reaction was stopped by adding 3,5-dinitrosalicylic acid (DNS) and

Table 1. Crystal data and structure refinement.

	[Cu(L)(2imi)] (**1**)	[Ni(L)(2imi)]·MeOH (**2**)
Empirical formula	$C_{17}H_{14}ClCuN_3O_2$	$C_{18}H_{18}ClN_3NiO_3$
Formula weight	391.31	418.51
Temperature	296(2) K	296(2) K
Wavelength	0.71073 Å	0.71073 Å
Crystal system	Monoclinic	Orthorhombic
Space group	$P2_1/c$	$P2_12_12_1$
Unit cell dimensions	a = 16.8758(9) Å	a = 4.54770(10) Å
	b = 10.8835(7) Å	b = 14.9634(3) Å
	c = 8.8026(5) Å	c = 26.8683(6) Å
	β = 100.030(3)°	β = 90°
Volume	1592.04(16) Å^3	1828.36(7) Å^3
Z	4	4
Density (calculated)	1.633 Mg m^{-3}	1.520 Mg m^{-3}
Absorption coefficient	1.554 mm^{-1}	1.230 mm^{-1}
F(0 0 0)	796	864
θ Range for data collection	1.23°–28.07°	1.52°–28.17°
Index ranges	$-22 \le h \le 22$	$-6 \le h \le 6$
	$-14 \le k \le 14$	$-19 \le k \le 19$
	$-11 \le l \le 11$	$-35 \le l \le 35$
Reflections collected	52,915	74,371
Independent reflections	3868 [R(int) = 0.0377]	4453 [R(int) = 0.0636]
Reflections observed (>2σ)	3298	3603
Data completeness	0.996	0.997
Refinement method	Full-matrix least-squares on F^2	Full-matrix least-squares on F^2
Data/restraints/parameters	3868/0/218	4453/0/237
Goodness-of-fit on F^2	0.813	1.109
Final R indices [$I > 2\sigma$ (I)]	R_1 = 0.0249	R_1 = 0.0369
	wR_2 = 0.0735	wR_2 = 0.0885
R indices (all data)	R_1 = 0.0330	R_1 = 0.0551
	wR_2 = 0.0847	wR_2 = 0.1077
Absolute structure parameter		−0.01(2)
Largest diff. peak and hole (e Å^{-3})	0.331 and −0.287	0.481 and −0.263

the amount of reducing sugars released was determined by dinitrosalicylic acid method [26]. One unit of α-amylase activity is defined as the amount of enzyme that produces reducing sugar equivalent to 1 µM maltose (as the standard) per minute under the assay conditions. A maltose standard curve was constructed with different concentrations of maltose. Furthermore, SDS-PAGE electrophoresis was performed using 10% acrylamide gel and then coomassie brilliant blue staining was performed according to the Laemmli method [27]. The protein concentration was determined by the Bradford assay using BSA as the standard [28]. Steady–state kinetic parameters K_m, V_{max}, and k_{cat} for immobilized enzyme were determined and compared with the free enzyme.

2.7. *Effect of chemical compounds on the amylolytic activity*

To investigate the effects of H_2L and its complexes (**1** and **2**), these compounds were added to the reaction tube. Tris–HCl (20 mM) was used as the buffer and the pH was finally adapted to 7.4. After addition of starch as the substrate to the reaction, the enzyme activity was determined as described previously. The activity of the enzyme was determined as the initial activity (or 100% activity) before addition of the compounds.

2.8. *Enzyme inhibitory effect of compounds*

The effect of [Ni(L)(2imi)]·MeOH enzyme activity was determined using the standard assay in the presence of 1–5 mM of these compounds as inhibitors and the type of inhibition for enzyme was determined by Lineweaver–Burk plots. One of the ways in which inhibition of enzyme-catalyzed reactions can be discussed is in terms of a general scheme is shown below:

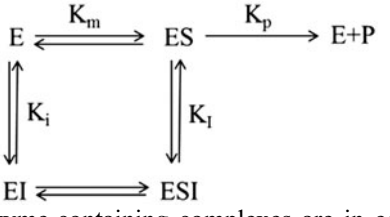

It is assumed that the enzyme-containing complexes are in equilibrium with each other, i.e. that the breakdown of ES in order to generate product does not significantly disturb the equilibrium [29, 30].

In the present work, all data obtained for a particular system were analyzed using a mixed model of enzyme inhibition as described in the following equation:

$$\frac{1}{V_0} = \frac{K_m(1 + ([I_0]/K_i))}{V_{max}} \frac{1}{[S_0]} + \frac{(1 + ([I_0]/K_I))}{V_{max}}$$

where V_0 is the initial reaction rate, V_{max} the maximum reaction rate, K_m the binding constant for the starch, and K_i and K_I are the inhibition constants for binding of inhibitor to enzyme and enzyme-substrate complex, respectively. In this model, a mixed inhibitor displays finite but unequal affinity for both the free enzyme and the ES complex; hence, the dissociation constants from each of these enzyme forms must be considered in the kinetic analysis of these inhibitors. I_0 and K_I were determined using secondary plots as described by the following equation:

$$\frac{1}{V'_{max}} = \frac{1 + \left(\frac{[I_0]}{K_I}\right)}{V_{max}}$$

Slope for inhibited reaction = slope for uninhibited reaction × $(1 + [I_0]/K_i)$. Hence, a secondary plot of $1/V_{max}$ against $[I_0]$ will be linear and the intercept on the $[I_0]$ axis gives $-K_I$. A graph of slope of primary plot against $[I_0]$ will also be linear and the intercept on the $[I_0]$ axis would be $-K_i$ [29, 30].

2.9. *Fluorescence measurements in the absence and presence of [Ni(L)(2imi)]·MeOH*

The intrinsic fluorescences of the native enzyme in the absence and presence of compounds were measured on a Perkin Elmer luminescence spectrometer LS 55. The excitation wavelength was set at 280 nm and the emission spectra were recorded from 300 to 400 nm. All experiments were carried out at room temperature with protein concentrations of 20 μM in 20 mM Tris buffer, pH 7.4.

2.10. *Antimicrobial activity*

Antibacterial assays were done on *Escherichia coli*, *Pseudomonas aeruginosa*, and *Agrobacterium tumifaciens* by Agar and broth dilution methods. Luria Bertani (LB) broth/agar medium was used to cultivate bacteria. A fresh overnight culture of inoculum of each culture was prepared [31]. The standardization of the bacterial cell number used for susceptibility testing is of critical importance for obtaining correct and reproducible results. For this reason, McFarland 0.5 $BaSO_4$ turbidity standard was used. Sterile paper disks of 4 mm diameter with increasing amount of [H_2L] or [Cu(L)(2imi)] and [Ni(L)(2imi)]·MeOH compounds in each disk were used for the antimicrobial assay in solid medium. Furthermore, bacteria are inoculated into a liquid growth medium in the presence of different concentrations of compounds as an antimicrobial agent.

3. Results and discussion

Schematic diagram for synthesis of [Cu(L)(2imi)] and [Ni(L)(2imi)]·MeOH complexes are presented in figure 1. This ligand has two main tautomeric forms. The title complexes were obtained in yields of 56–64%. They are insoluble in water and *n*-hexane, partially soluble in common organic solvents and have excellent solubility in DMF and DMSO. These complexes showed non-electrolyte behavior in DMSO (10^{-3} M).

3.1. *Spectral characterizations*

Selected frequencies and vibrational assignments are listed in the Experimental section. In the spectrum of H_2L, strong absorption at 1627 cm^{-1} is related to ν(C=N) which shows a red shift after coordination, indicating that coordination takes place through the azomethineic nitrogen [32]. In the spectrum of ligand, the band at 1307 cm^{-1} is due to the CO vibration that exhibits 26 and 23 cm^{-1} shifts to lower frequencies upon complexation.

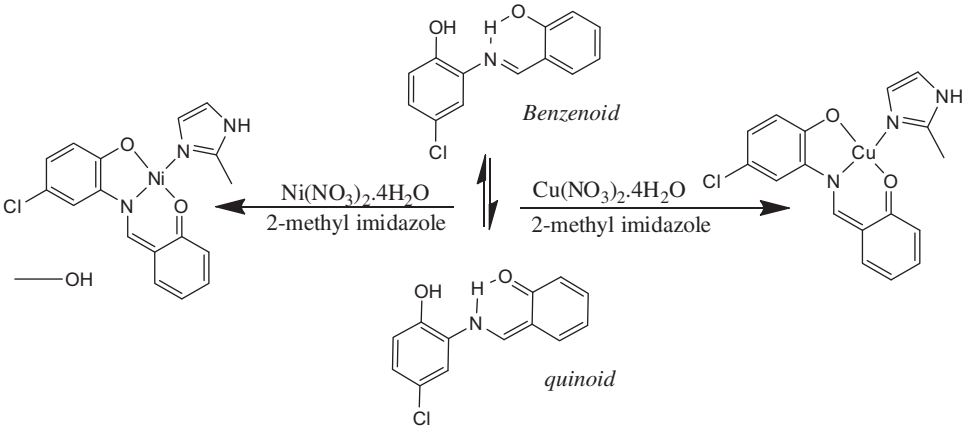

Figure 1. Schematic diagram for complexation processes.

These shifts indicate the ligand is coordinated to metal ion through phenolic oxygens in both complexes [33]. Bands due to NH stretch are assigned at 3421 cm^{-1} for **1** and 3421 cm^{-1} for **2** [34]. Finally, the OH band vibrations of non-coordinated methanol in [Ni(L)(2imi)]·MeOH are at 3101 cm^{-1} [35].

The electronic spectra of H_2L and its complexes were recorded in DMSO. According to our previous work [22], in the UV–vis spectrum of H_2L, a band at 268 nm corresponds to $\pi \rightarrow \pi^*$ transitions of aromatic rings. The azomethine $\pi \rightarrow \pi^*$ and $n \rightarrow \pi^*$ transitions are assigned at 350 and 438 nm, respectively [22]. In the electronic spectra of complexes, all the bands shift in comparison with free ligand, indicating coordination of Schiff base [33]. In the Ni(II) complex, the band at 450 nm may be due to LMCT (O/N(p)→Ni(d)) transition and in case of Cu(II) complex, the band at 450 nm with the epsilon value of loge = 3.06 is due to admixture of LMCT and MLCT. Moreover, **1** with d^9 and **2** with d^8 electron configuration in square planar geometry have three transitions. These transitions for **1** are $^2A_{1g} \rightarrow {}^2B_{1g}$, $^2B_{2g} \rightarrow {}^2B_{1g}$, and $^2E_g \rightarrow {}^2B_{1g}$ and for **2** are $^1A_{1g} \rightarrow {}^1A_{2g}$, $^1A_{1g} \rightarrow {}^1B_{1g}$, and $^1A_{1g} \rightarrow {}^1E_g$. The tailing of CT bands for **1** and **2** to the visible region causes the disappearance of these bands and only the $^2E_g \rightarrow {}^2B_{1g}$ transition at 661 nm for [Cu(L)(2imi)] [36].

3.2. *X-ray crystal structures*

In **1** and **2,** 2-(((5-chloro-2-oxyphenyl)imino)methyl)phenolato) behaves as a dianionic tridentate ligand, coordinating through two phenolate oxygens and the imino nitrogen (ONO donor). Coordination of the metal (Cu or Ni) is completed with monodentate 2-methyl imidazole. The coordination around both metals is square planar and the Schiff base is essentially planar. ORTEP drawings of both compounds are given in figures 2 and 3, and selected geometrical parameters are gathered in table 2.

The coordination behavior of the Schiff base is similar to that previously found in similar nickel [37, 38] or copper complexes, with [CuO_2N_2] core [39–41] or even with [CuO_2N_3]

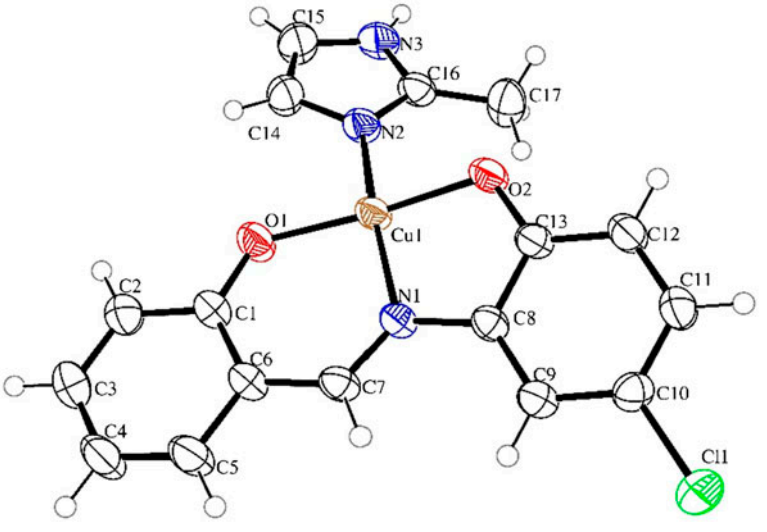

Figure 2. ORTEP diagram of **1**.

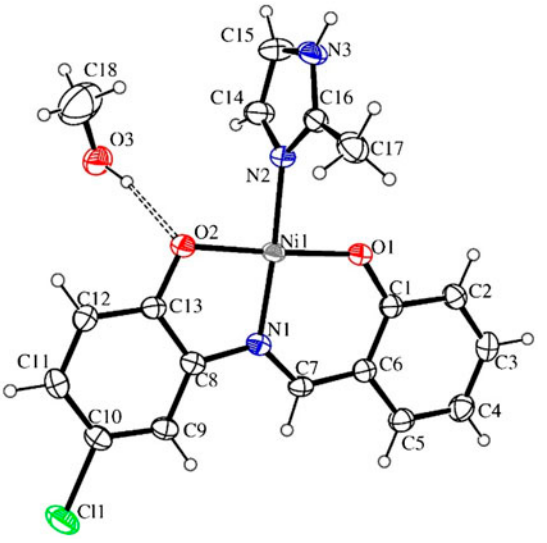

Figure 3. ORTEP diagram of **2**.

Table 2. Selected bond lengths (Å) and angles (°).

	[Cu(L)(2imi)]	[Ni(L)(2imi)]·MeOH
M*–O(1)	1.8827(13)	1.822(2)
M–O(2)	1.9293(13)	1.864(2)
M–N(1)	1.9460(14)	1.857(3)
M–N(2)	1.9940(15)	1.906(3)
O(1)–M–N(1)	93.55(6)	95.94(11)
O(2)–M–N(1)	84.50(6)	86.45(11)
O(1)–M–N(2)	88.82(6)	88.04(11)
O(2)–M–N(2)	95.54(6)	89.56(11)
∑*cis* angles	362.41	359.99
O(1)–M–O(2)	168.34(7)	177.35(11)
N(1)–M–N(2)	167.60(6)	175.95(13)
∑*trans* angles	335.94	353.3
Total sum	698.35	713.29

*M=Cu for [Cu(L)(2imi)] and Ni in case of [Ni(L)(2imi)]·MeOH.

core (five coordinate) [35, 42]. In **1**, the Cu–N distances are 1.9464(15) and 1.9936(16) Å and the Cu–O distances are 1.8834(13) and 1.9296(13) Å. Cu–O distances are clearly shorter than those found in [Cu(Br-SAA)(ImH)] [41]. The Cu–N(imi) bond length in **1** is longer than Cu–N(1), contrasting to [Cu(Br-SAA)(ImH)] [41], where both bond distances are equal. In **2**, the Ni–N distances are 1.857(3) and 1.906(3) Å, in fact, same values that were found for imidazole(2-((5-chloro-2-hydroxyphenylimino)methyl)phenolato)nickel(II) [38]. The Ni–O bond lengths are 1.822(2) and 1.865(2) Å, values also similar to those in the aforementioned complex.

In **1** and **2**, coordination of the tridentate Schiff base generates a four cycle fused system, two phenolates at both ends and, in the middle, two metallacycles, one five-membered and

the other one six-membered. The four cycle fused system is planar, although the copper complex is much more distorted than the nickel one, as demonstrated by the dihedral angle between the phenolate rings, 12.19(10)° for [Cu(L)(2imi)] and only 4.77 (17)° for [Ni(L)(2imi)]·MeOH. The dihedral angle between metallacycles is 9.51(7)° for **1** and only 3.13(13)° for **2**.

The metal core [N_2O_2] is also much more distorted for **1** than in **2**. The *trans* angles, for example, are 168.36(7) and 167.61(6)° in [Cu(L)(2imi)], clearly deviating from 180°. In the case of [Ni(L)(2imi)]·MeOH, those values are almost 180° [177.35(11) and 175.95(13)°]. This is in contrast with the [Cu(Br-SAA)(ImH)] [41] with *trans* angles over 173.4(2)°(figure 4).

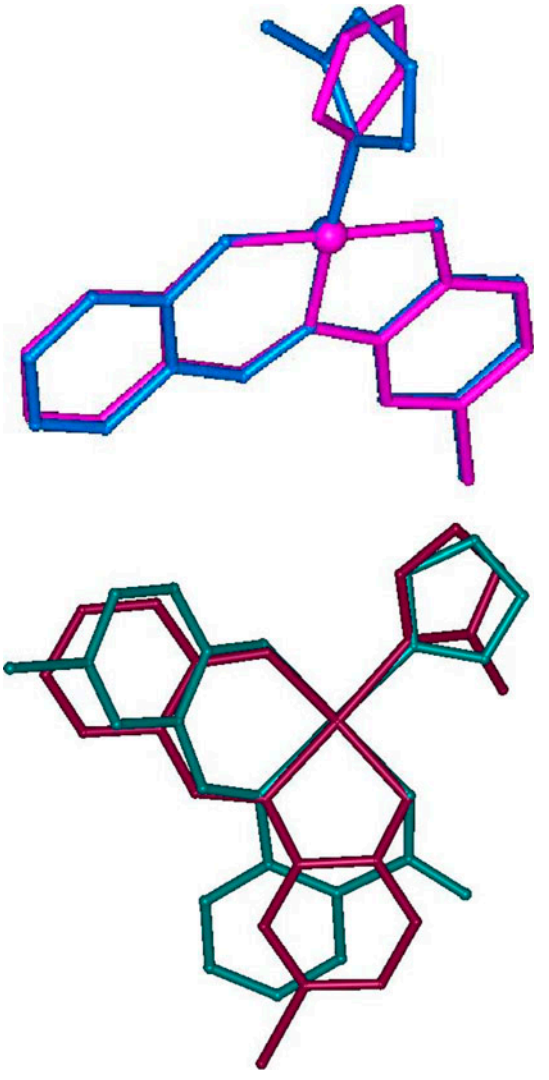

Figure 4. Upper: comparative figure between [Ni(L)(2imi)] (blue) and [Ni(L)(imi)] [38] (pink). Lower: comparative figure between [Cu(L)(2imi)] (red) and [Cu(Br-SAA)(ImH)] [41] (green) (see http://dx.doi.org/10.1080/00958972.2014.1000883 for color version).

The distortion in the core can be evaluated through the sum of the angles in the coordination sphere. In a perfect square planar geometry, the sum of the *cis* angles should be 360°, and also the sum of *trans* angles should be 360°. The sum of both values (720°) could be used for comparison with a tetrahedral core, where the sum of the six angles (109.47°) should be 656.82 [43, 44]. For [Cu(L)(2imi)], the sum of those values is 698.38, whereas for [Ni(L)(2imi)]·MeOH, such sum resulted to be 713.29°. These values clearly indicate that the copper complex is somewhat distorted towards a tetrahedral geometry, while the nickel complex shows a square-planar geometry scarcely distorted.

The neutral 2-methyl imidazole behaves differently in the two compounds. In **1**, neutral imidazole is not in the plane, but forms a dihedral plane with the donor atom plane of 27.44(10)°. However, in **2**, this ligand is almost perpendicular, with a dihedral angle of 76.5 (2). The angle between the Cu–N(2) vector and the coordination plane is 5.86(7)°, as a consequence of the mentioned distortion, while the corresponding angle between the Ni–N(2) vector and the $[N_2O_2]$ plane is only 0.37(12)°. This disposition is quite different from that found in the non-substituted imidazole complex [38] as shown in figure 4, indicating that the presence of the methyl group in the ligand determines the disposition of this ligand. The neutral 2-methyl imidazole ligand plays an important role in the supramolecular structure of both compounds. In the case of **1**, a classical N–H···O hydrogen bond is formed between neighboring molecules, as shown in figure 5, with the parameters found in table 3. This interaction causes a zig-zag growing in the *z* axis. Those 1-D zigzag structures are ordered in the unit cell as shown in figure 6; figure 7 shows the unit cell for [Cu(L)(2imi)].

In the case of **2**, the asymmetrical unit contains, in addition to the complex, also a methanol, not coordinated, that plays an important role in the supramolecular network. Indeed, a classical O–H···O hydrogen bond is formed between methanol and one coordinating oxygen of a phenolate. Once more, the non-coordinating NH group of 2-methyl imidazole forms a

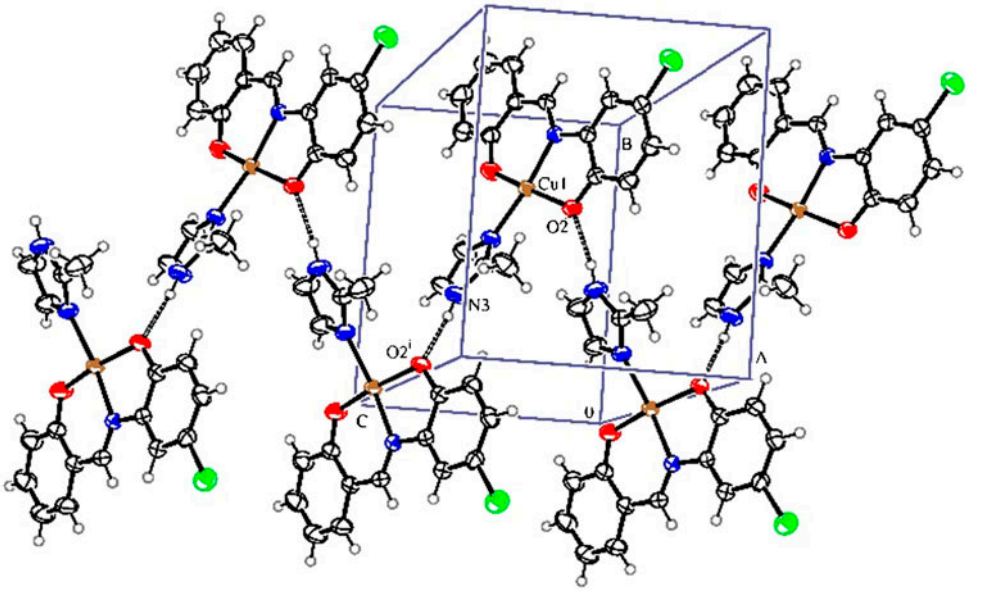

Figure 5. Growing of [Cu(L)(2imi)] along the *z* axis.

Table 3. Hydrogen bonds for [Cu(L)(2imi)] (Å and °).

D–H···A	*d*(D–H)	*d*(H···A)	*d*(D···A)	∠(DHA)
N(3)–H···O(2^{i})	0.86	1.92	2.771(2)	169.3

Note: Symmetry transformations used to generate equivalent atoms, i: x, $1/2 - y$, $1/2 + z$.

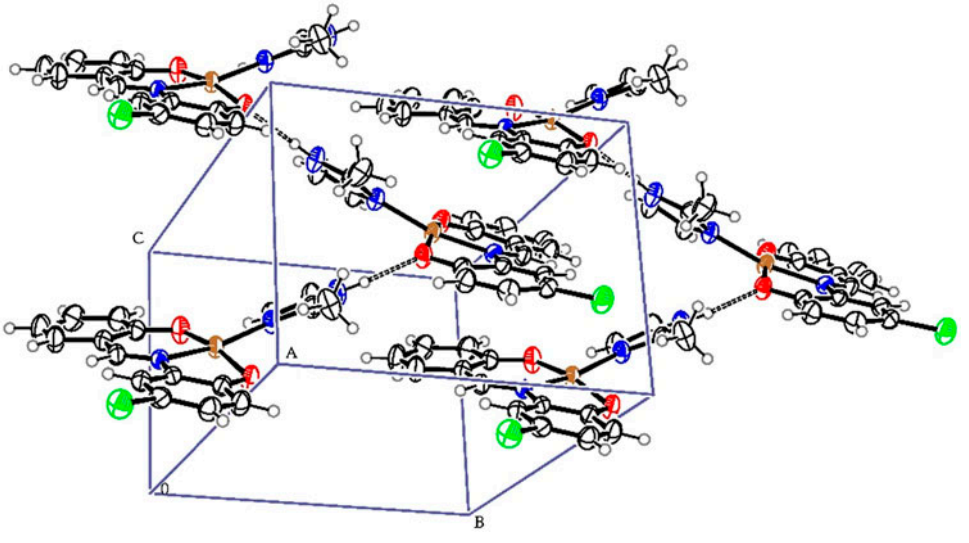

Figure 6. The 1-D zigzag arrangement.

classical N–H···O hydrogen bond with methanol, similar to that found in imidazole(2-((5-chloro-2-hydroxyphenylimino)methyl)phenolato)nickel(II) [38]. Thus, the methanol is implicated in two hydrogen bonds as shown in figure 8, with the hydrogen bond parameters in table 4.

The disposition of the 2-methyl imidalole ring, almost perpendicular to the plane containing the rest of the molecule (metal + Schiff base) (*vide supra*) allows a C–H-π interaction, whose parameters are shown in table 5 (figures 9 and 10).

3.3. *Kinetic parameters determination*

The kinetic parameters of the enzyme were determined in the absence and presence of **1** as described above. The K_m of the enzyme was calculated from a Lineweaver–Burk plot and the results compared to those obtained for the control without complex (figure 11). The K_m values were estimated as 3 and 4 mM for enzyme in the absence and presence of complex, respectively, with a 1.3-fold decrease in K_m for **1**. Reduction of K_m reflects the change made in molecular recognition of the substrate by enzyme. This alteration was either due to slight conformational changes of the enzyme in the presence of **1**, resulting in a lower possibility of forming a substrate–enzyme complex, or lower accessibility of the substrate to the active sites of the enzyme. The presence of Ni has a slight effect on the enzyme catalysis accompanied with a decrease of K_m.

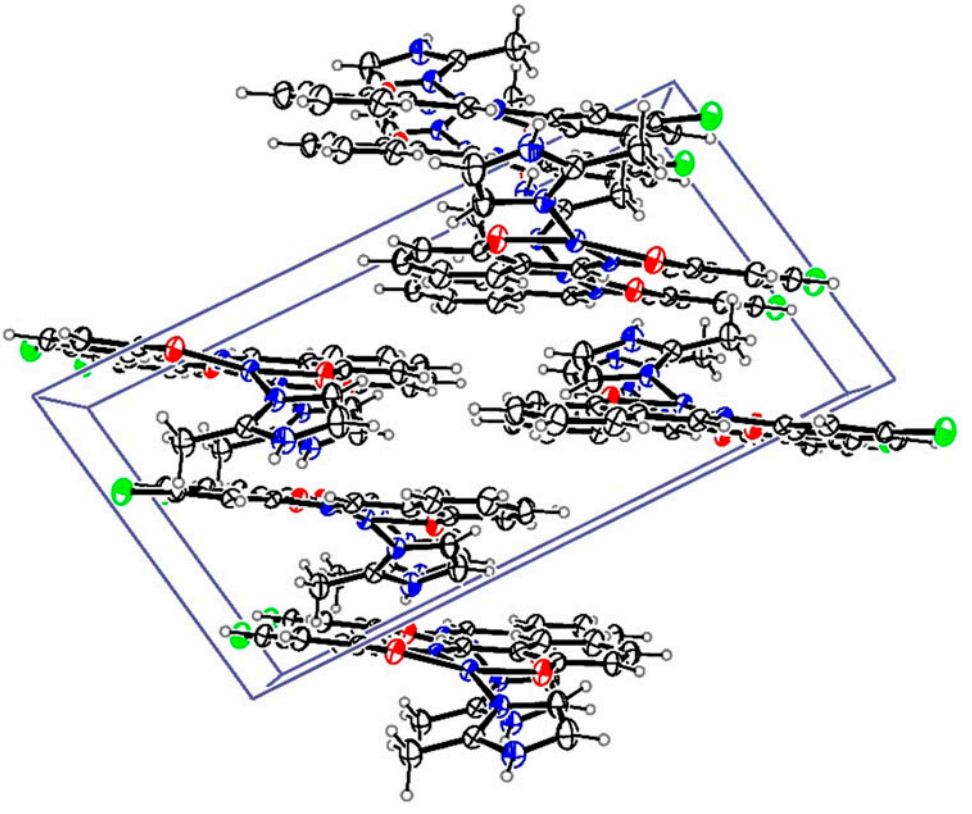

Figure 7. Unit cell for [Cu(L)(2imi)].

3.4. *Inhibition of amylase by [Ni(L)(2imi)]·MeOH*

The enzyme activity was measured in the presence of **1** and **2** at 37 °C as shown in table 6. [Cu(L)(2imi)] (2 mM) had no effect on α-amylase activity, but in the presence of [Ni(L)(2imi)]·MeOH (2 and 5 mM) an inhibitory effect was detected. To investigate the mechanism of action of [Ni(L)(2imi)]·MeOH complex, we used this compound in reaction mixture. Reaction rates were determined for different substrate concentrations using enzyme, and measurements were carried out in the presence of **2** as the inhibitor. Enzyme deactivation or enzyme inhibition was assumed to be the reason for the observed reduction in enzyme activity. The activity was recovered by dilution and remained constant during the incubation time indicating reversible inhibition and showed mixed inhibition patterns (figure 12). A mixed inhibitor displays affinity for both the free enzyme and the enzyme–substrate complex. Mixed-type inhibitors interfere with substrate binding and hamper catalysis in the ES complex. Since there is no structural similarity between these compounds and substrate, it is likely that this inhibitor interacts with the enzyme at a site separate from the substrate binding sites.

The structure changes using intrinsic fluorescence measurements were recorded to study protein unfolding/denaturation at concentrations of compounds where inhibition occurs. Denaturation was followed by both changes in the maximal intensity of fluorescence (I_{max})

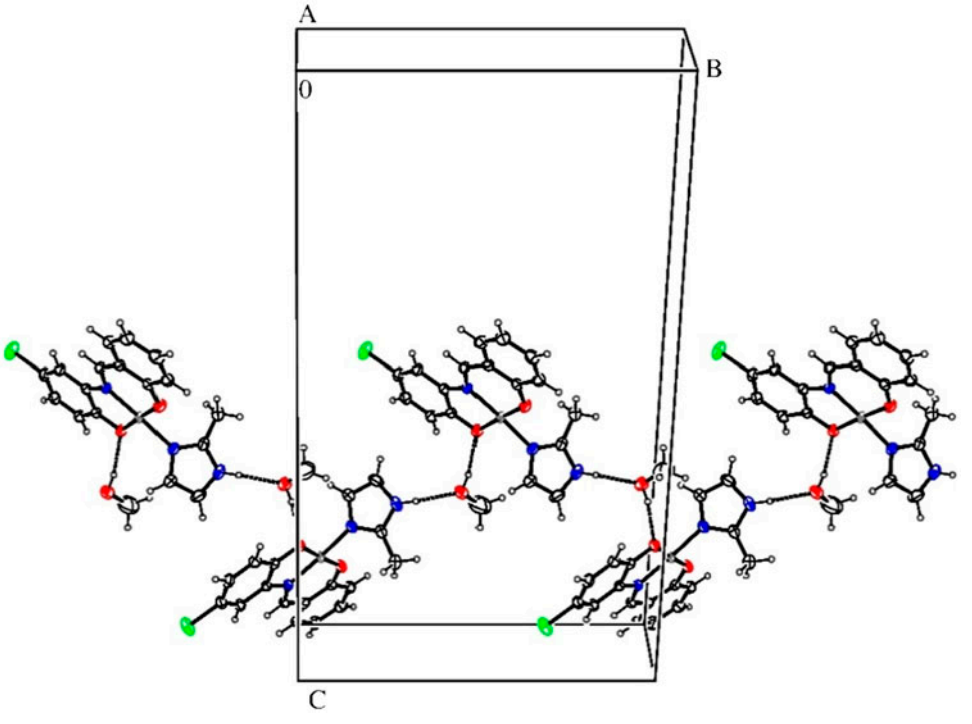

Figure 8. Growing of [Ni(L)(2imi)]·MeOH along the *y* axis.

Table 4. Hydrogen bonds for [Ni(L)(2imi)]·MeOH (Å and °).

D–H···A	*d*(D–H)	*d*(H···A)	*d*(D···A)	∠(DHA)
N(3)–H(3A)···O(3^{i})	0.86	1.97	2.807(4)	163
O(3)–H(3B)···O(2)	0.82	1.91	2.716(4)	169

Note: Symmetry transformations used to generate equivalent atoms, i: $2 - x$, $1/2 + y$, $3/2 - z$.

Table 5. C–H-π interaction parameters for [Ni(L)(2imi)]·MeOH (Å and °).

Interaction	H···Ct	H-Perp	γ	∠(X–H···Ct)	X···Ct	∠(X–H, π)
C(17)–H(17C)···Ct1	2.74	2.71	8.02	138	3.508(5)	55

Notes: γ is the angle between Ct–H vector and ring normal.
Symmetry transformations used to generate equivalent atoms, 1: $x - 1$, y, z.

and the red shift of the maximal emission wavelength (λ_{max}). As shown in figure 13, the intrinsic fluorescence of enzyme in the presence of increased concentration of [Ni(L)(2imi)]·MeOH was lower than the native enzyme. Fluorescence emission of a protein is the result of its intrinsic fluorophores like Trp and Tyr residues. The intensity of emission is related to the protein conformation which may expose, or bury, the internal fluorophores.

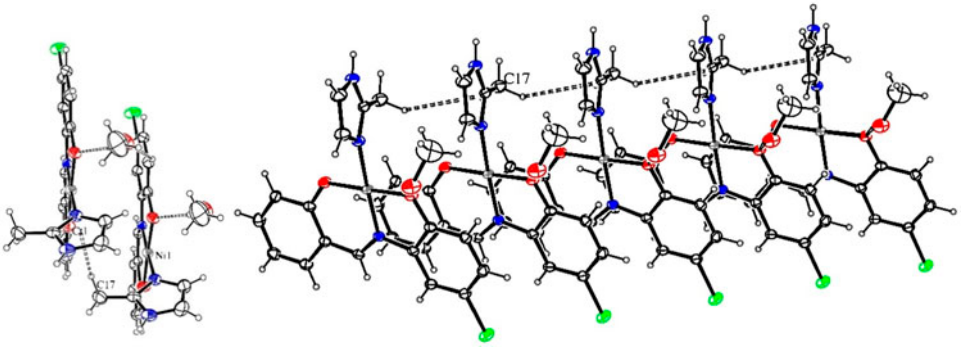

Figure 9. Growing of [Ni(L)(2imi)]·MeOH in the *x* axis due a C–H-π interaction.

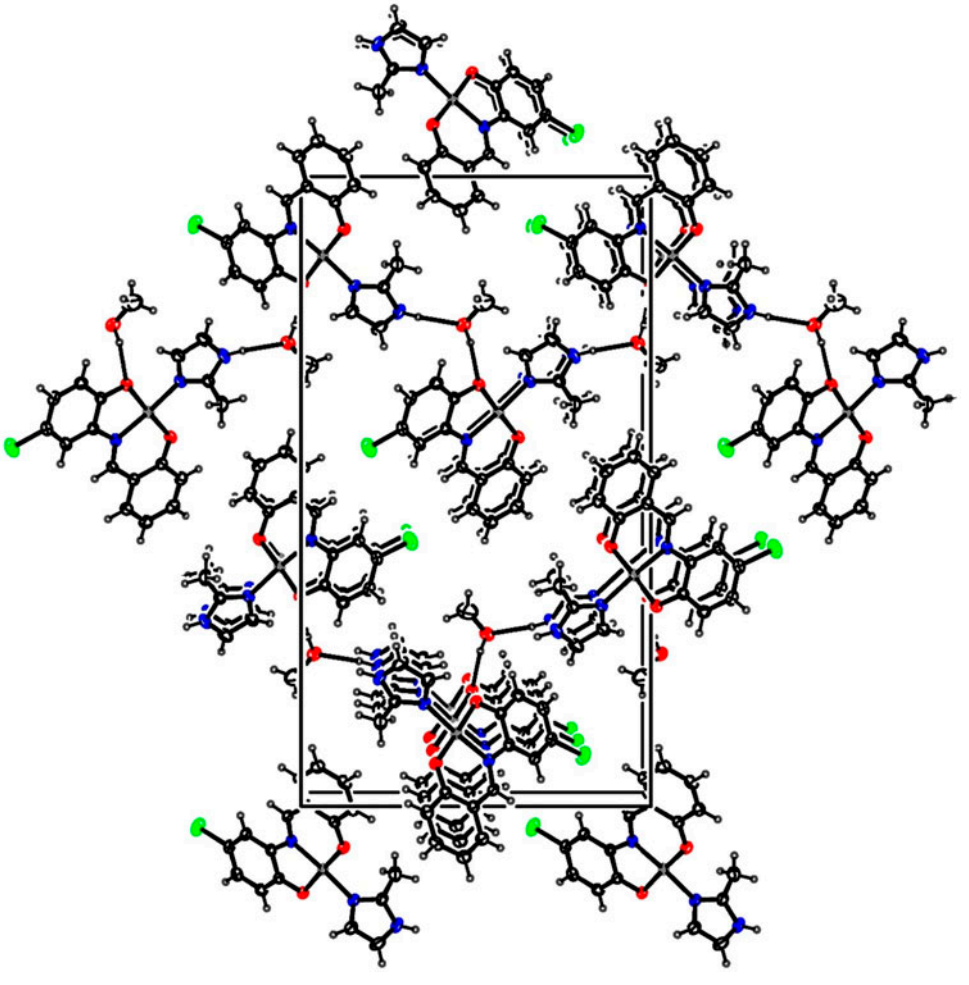

Figure 10. Unit cell for [Ni(L)(2imi)]·MeOH.

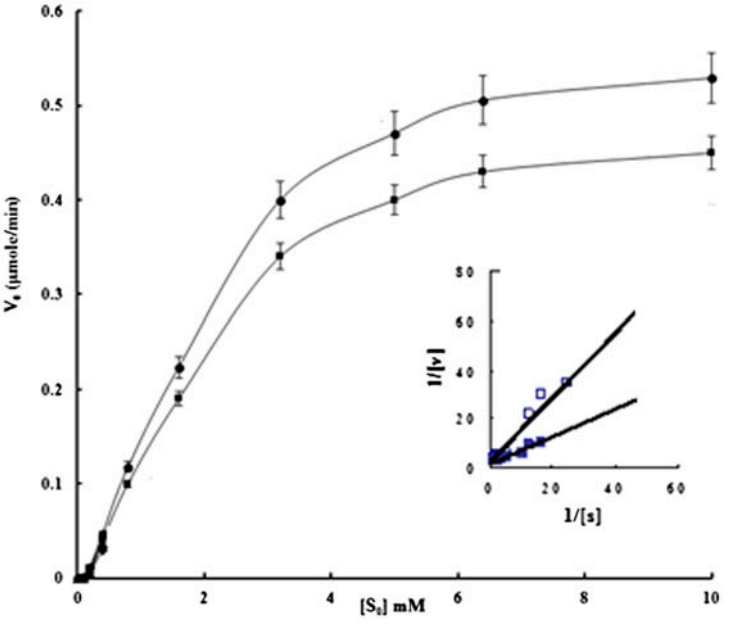

Figure 11. The Michaelis–Menten diagram of enzyme in the absence (●) and presence (■) of **1**. Inset: Lineweaver–Burk plots.

Table 6. The effect of metal ions and some reagents on enzyme activity.

Compounds	Relative activity (2 mM)	Relative activity (5 mM)
Control (no addition)	1.00	1.00
H_2L	0.88	0.85
[Cu(L)(2imi)]	1.00	0.86
[Ni(L)(2imi)]·MeOH	0.8	0.6

3.5. *Antimicrobial activity*

To test the antimicrobial properties for the compounds, we used cultured pathogenic bacteria. The antimicrobial activity was assayed on LBA plates and liquid medium using the agar and broth dilution methods. Different amounts of H_2L, [Cu(L)(2imi)] and [Ni(L)(2imi)]·MeOH were placed on the disks and the inhibition zones of the different pathogenic microbes were measured. As seen in table 7, activity of the Cu(II) complex against all tested microorganisms was greater than the other compounds. This enhancement in activity may be due to an efficient diffusion of the complex into the cell and/or interaction with the cell [45]. For the Ni(II) complex, higher antifungal activity was observed against *Aspergillus fumigatus* than the ligand, but the antibacterial activity of the ligand was more than that of the Ni(II) complex.

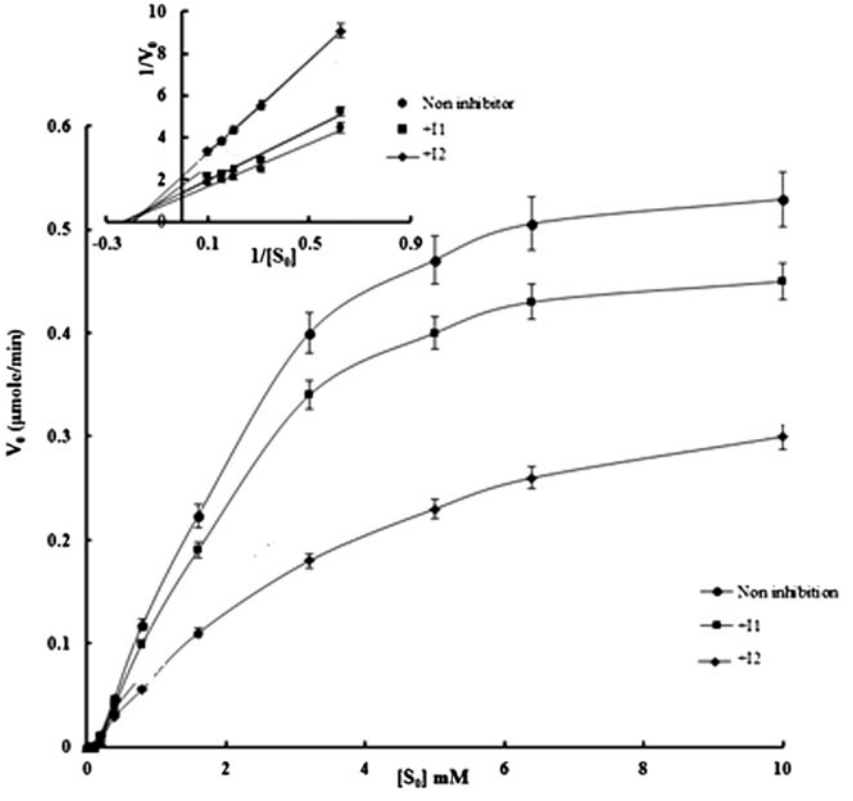

Figure 12. Michaelis–Menten and Lineweaver–Burk plots related to alpha amylase inhibition at different concentrations of **2**. Concentration of the enzyme in all experiments is 20 µg ml^{-1}. $1/v$ is the reciprocal initial velocity in unit^{-1}. Standard deviations were within 5% of the experimental values.

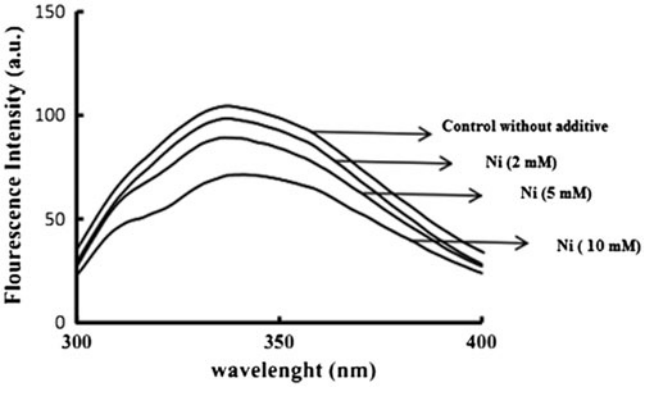

Figure 13. Structural modification analysis of the enzyme in the absence and presence of **2** using intrinsic fluorescence. Fluorescence intensities of enzyme were decreased in the presence of different concentration of **2** in comparison to control (Ni = [Ni(L)(2meimi)]·MeOH).

Table 7. Antimicrobial activity in the presence of H_2L and its complexes.

Compounds	*A. tumefaciens*	*P. aeruginosa*	*E. coli*	*S. pneumonia*	*A. fumigatus*
H_2L (30 ppm)	Intermediate (14 mm)	Intermediate (13.5 mm)	Sensitive (24 mm)	Intermediate (16 mm)	Resistance (10 mm)
[Cu(L)(2imi)] (30 ppm)	Sensitive (26.5 mm)	Intermediate (17 mm)	Sensitive (22 mm)	Sensitive (20 mm)	Intermediate (19.5 mm)
[Ni(L)(2imi)]·MeOH (30 ppm)	Intermediate (18 mm)	Resistance (13 mm)	Resistance (11 mm)	Resistance (10 mm)	Intermediate (16 mm)
Chloramphenicol	Sensitive (18.5 mm)	Sensitive (18 mm)	Sensitive (22 mm)	Sensitive (21 mm)	Intermediate (16 mm)
Vancomycin	Sensitive (16 mm)	Sensitive (18 mm)	Intermediate (11 mm)	Resistance (6 mm)	Sensitive (19 mm)

4. Conclusion

In this study, two new Cu(II) and Ni(II) complexes were synthesized and characterized using spectroscopic techniques. Both complexes have square planar geometry, from donors of Schiff base ligand and nitrogen of 2-methyl imidazole. Biochemical activities of **1** and **2** were also investigated. Furthermore, the effects of H_2L, [Cu(L)(2imi)] and [Ni(L)(2imi)]·MeOH upon α-amylase activity were carried out and biochemical characterization of enzyme in the presence of the compounds was determined. Results showed a 1.3-fold decrease in K_m value for [Cu(L)(2imi)]. The experimental data showed that α-amylase was inhibited by the [Ni(L)(2imi)]·MeOH. The reciprocal plot related to the reversible inhibitory effect of inhibitor showed mixed inhibition patterns. According to the antimicrobial results, the [Cu(L)(2imi)] shows more activity against all bacterial varieties in comparison to [Ni(L)(2imi)]·MeOH and H_2L.

Supplementary material

CCDC 961113 and 961114 contain the supplementary crystallographic data for **1** and **2**, respectively. A copy of this information may be obtained free of charge from The Director, CCDC, 12 Union Road, Cambridge, CB2 1EZ, UK (Fax: +44 1223 336 033); web page: http://www.ccdc.cam.ac.uk/cgi-bin/catreq.cgi.

Acknowledgements

Authors gratefully acknowledge the financial support provided for this work by the Shahid Bahonar University of Kerman. We thank the University of Messina for provision of the diffractometer.

References

[1] A. Ünal, B. Eren, E. Eren. *J. Mol. Struct.*, **1049**, 303 (2013).
[2] A. Cinarli, D. Gürbüz, A. Tavman, A.S. Birteksöz. *Chinese J. Chem.*, **30**, 449 (2012).
[3] S. Anbu, M. Kandaswamy. *Polyhedron*, **30**, 123 (2011).
[4] A. Gorczyński, M. Wałęsa-Chorab, M. Kubicki, M. Korabik, V. Patroniak. *Polyhedron*, **77**, 17 (2014).

[5] J.R. Davis. *ASM International Handbook Committee, Nickel Cobalt and Their Alloys*, ASM International, Ohio, OH (2000).
[6] J.R. Davis. *ASM International Handbook Committee, Copper and Copper Alloys*, ASM International, Ohio, OH (2001).
[7] P. Noblía, E.J. Baran, L. Otero, P. Draper, H. Cerecetto, M. González, O.E. Piro, E.E. Castellano, T. Inohara, Y. Adachi, H. Sakurai, D. Gambino. *Eur. J. Inorg. Chem.*, **2004**, 322 (2004).
[8] J.H. McNeill, V.G. Yuen, S. Dai, C. Orvig. *Mol. Cell. Biochem.*, **153**, 175 (1995).
[9] G. Floris, B. Mondovi. *Copper Amine Oxidases: Structures, Catalytic Mechanisms and Role in Pathophysiology*, Taylor & Francis, London (2009).
[10] R. Crichton. *Biological Inorganic Chemistry: An Introduction*, Elsevier Science, Oxford (2007).
[11] L.T. Tran, C.P. Constabel. *Planta*, **234**, 799 (2011).
[12] V.A. Joseph, K.M. Vyas, J.H. Pandya, V.K. Gupta, R.N. Jadeja. *J. Coord. Chem.*, **66**, 1094 (2013).
[13] S. Thalamuthu, B. Annaraj, S. Vasudevan, S. Sengupta, M.A. Neelakantan. *J. Coord. Chem.*, **66**, 1805 (2013).
[14] M.-J. Niu, D.-W. Sun, H.-H. Li, Z.-Q. Cao, S.-N. Wang, J.-M. Dou. *J. Coord. Chem.*, **67**, 81 (2014).
[15] P. Kavitha, M. Saritha, K. Laxma Reddy. *Acta, Part A*, **102**, 159 (2013).
[16] M.A. Farrugia, L. Macomber, R.P. Hausinger. *J. Biol. Chem.*, **288**, 13178 (2013).
[17] A.A. Abdel Aziz, A.N.M. Salem, M.A. Sayed, M.M. Aboaly. *J. Mol. Struct.*, **1010**, 130 (2012).
[18] S. Celen, E. Gungor, H. Kara, A.D. Azaz. *J. Coord. Chem.*, **66**, 3170 (2013).
[19] V.B. Badwaik, R.D. Deshmukh, A.S. Aswar. *J. Coord. Chem.*, **62**, 2037 (2009).
[20] V.B. Rodríguez, E.J. Alameda, J.F. Martínez Gallegos, A.R. Requena, A.I. García. *Biochem. Eng. J.*, **27**, 299 (2006).
[21] O.L. Franco, D.J. Rigden, F.R. Melo, C. Bloch Jr., C.P. Silva, M.F. Grossi de Sá. *Eur. J. Biochem.*, **267**, 2166 (2000).
[22] S.Y. Ebrahimipour, M. Abaszadeh, J. Castro, M. Seifi. *Polyhedron*, **79**, 138 (2014).
[23] (a) *COSMO*, Bruker AXS Inc., Madison, WI (2005); (b) *SAINT (Version 7.06A)*, Bruker AXS Inc., Madison, WI (2005); (c) *SADABS (Version 2.10)*, Bruker AXS Inc., Madison, WI (2005).
[24] M.C. Burla, R. Caliandro, M. Camalli, B. Carrozzini, G.L. Cascarano, L. De Caro, C. Giacovazzo, G. Polidori, R. Spagna. *J. Appl. Crystallogr.*, **38**, 381 (2005).
[25] G.M. Sheldrick. *Acta Crystallogr. A.*, **64**, 112 (2008).
[26] G.L. Miller. *Anal. Chem.*, **31**, 426 (1959).
[27] U.K. Laemmli. *Nature*, **227**, 680 (1970).
[28] M.M. Bradford. *Anal. Biochem.*, **72**, 248 (1976).
[29] R.A. Copeland. *Enzymes: A Practical Introduction to Structure, Mechanism, and Data Analysis*, 2nd Edn, Wiley, New York (2004).
[30] N.C. Price, L. Stevens. *Enzyme Technology, Fundamentals of Enzymology: The Cell and Molecular Biology of Catalytic Proteins*, 3rd Edn, Oxford University Press, Oxford (1999).
[31] I. Wiegand, K. Hilpert, R.E. Hancock. *Nat. Protoc.*, **3**, 163 (2008).
[32] (a) S.Y. Ebrahimipour, I. Sheikhshoaie, A. Crochet, M. Khaleghi, K.M. Fromm. *J. Mol. Struct.*, **1072**, 267 (2014); (b) S.Y. Ebrahimipour, H. Khabazadeh, J. Castro, I. Sheikhshoaie, A. Crochet, K.M. Fromm. *Inorg. Chim. Acta*, **427**, 52 (2015).
[33] S.Y. Ebrahimipour, J.T. Mague, A. Akbari, R. Takjoo. *J. Mol. Struct.*, **1028**, 148 (2012).
[34] I. Sheikhshoaie, S.Y. Ebrahimipour, M. Sheikhshoaie, H. Amiri Rudbari, M. Khaleghi, G. Bruno. *Acta, Part A*, **124**, 548 (2014).
[35] R. Takjoo, J.T. Mague, A. Akbari, S.Y. Ebrahimipour. *J. Coord. Chem.*, **66**, 2852 (2013).
[36] R. Takjoo, A. Akbari, M. Ahmadi, H. Amiri Rudbari, G. Bruno. *Polyhedron*, **55**, 225 (2013).
[37] M. Sari, O. Atakol, N. Yilmaz, D. Ülkü. *Anal. Sci.*, **15**, 401 (1999).
[38] R. Takjoo, A. Akbari, S.Y. Ebrahimipour, H. Amiri Rrudbari, G. Brunò. *C. R. Chimie*, **17**, 1144 (2014).
[39] K. Liu, G. Liu, Z. Cao, M. Niu. *Acta Crystallogr. E*, **66**, m78 (2009).
[40] A. Elmali, O. Atakol, I. Svoboda, H. Fuess. *Z. Kristallogr.*, **205**, 146 (1993).
[41] R.N. Patel. *Indian J. Chem.*, **48A**, 1370 (2009).
[42] E. Labisbal, J.A. Garcia-Vazquez, J. Romero, S. Picos, A. Sousa, A. Castiñeiras, C. Maichle-Mössmer. *Polyhedron*, **14**, 663 (1995).
[43] P.R. Raithby, G.P. Shields, F.H. Allen, W.D.S. Motherwell. *Acta Crystallogr. B*, **56**, 444 (2000).
[44] C. Lochenie, S. Schlamp, A.P. Railliet, K. Robeyns, B. Weber, Y. Garcia. *CrystEngComm*, **16**, 6213 (2014).
[45] Z.H. Chohan, C.T. Supuran, A. Scozzafava. *J. Enzyme Inhib. Med. Chem.*, **19**, 79 (2004).